Atmos. Chem. Phys. Discuss., 14, 17401–17438, 2014
www.atmos-chem-phys-discuss.net/14/17401/2014/
doi:10.5194/acpd-14-17401-2014

Atmospheric Chemistry and Physics
Discussions

Low temperatures enhance organic nitrate formation: evidence from observations in the 2012 Uintah Basin Winter Ozone Study

L. Lee[1], **P. J. Wooldridge**[1], **J. B. Gilman**[2], **C. Warneke**[2], **J. de Gouw**[2], **and R. C. Cohen**[1,3]

[1]Department of Chemistry, University of California, Berkeley, CA, USA
[2]Chemical Science Division, Earth System Research Laboratory, National Oceanic & Atmospheric Administration, Boulder, CO, USA
[3]Department of Earth and Planetary Sciences, University of California, Berkeley, CA, USA

Received: 28 May 2014 – Accepted: 10 June 2014 – Published: 30 June 2014

Correspondence to: R. C. Cohen (rccohen@berkeley.edu)

Published by Copernicus Publications on behalf of the European Geosciences Union.

Abstract

Nitrogen dioxide (NO_2) and total alkyl nitrates (ΣANs) were measured using thermal dissociation laser induced fluorescence during the 2012 Uintah Basin Winter Ozone Study (UBWOS) in Utah, USA. The observed NO_2 concentration was highest before sunrise and lowest in the late afternoon, suggestive of a persistent local source of NO_2 coupled with turbulent mixing out of the boundary layer. In contrast, ΣANs co-varied with solar radiation with a noontime maximum, indicating that local photochemical production combined with rapid mixing and/or deposition was the dominant factor in determining the ΣAN concentrations. We calculate that ΣANs were a large fraction ($\sim 60\,\%$) of the HO_x free radical chain termination and show that the temperature dependence of the alkyl nitrate yields enhances the role of ΣANs in local chemistry during winter by comparison to what would occur at the warmer temperatures of summer.

1 Introduction

The Uintah Basin in Utah is a region of concentrated fossil fuel extraction operations using hydraulic fracturing to extract natural gas and oil from shale formations. The basin has experienced high wintertime ozone as has the nearby Upper Green River Basin in Wyoming (Schnell et al., 2009). The observed ~ 200 ppb peak ozone in the basin during the winter of 2011 was associated with elevated concentrations of volatile organic compounds (VOCs) coincident with a shallow boundary layer stabilized by snow cover, which doubled as a solar reflector leading to more rapid photochemistry.

Organic nitrates ($RONO_2$) are products of atmospheric VOC oxidation in the presence of NO_x ($NO + NO_2$). During daytime, their formation involves the association reaction of alkyl peroxy radicals with NO. This reaction terminates ozone formation and suppresses OH recycling. The importance of $RONO_2$ formation as a NO_x sink and chain terminator of ozone production depends on the mixture of VOCs present as a result of variations in OH reactivity and organic nitrate yield, α, among different organic molecules (Perring et al., 2013; Farmer et al., 2011). Laboratory studies have shown that the nitrate yield follows standard expectations for 3-body reactions: α increases with carbon number of the organic peroxy radical and atmospheric pressure, but decreases with temperature (Atkinson et al., 1983; Carter and Atkinson, 1989). Field observations have found $RONO_2$ compounds to account for 25 % or more of total reactive nitrogen (NO_y, defined as NO_x + higher nitrogen oxides). However, none of these prior field experiments (Farmer et al., 2011; Rosen et al., 2004; Perring et al., 2010, 2009) covered a temperature range wide enough to examine the role of the temperature dependence of α on nitrate formation rates, O_3, or OH concentrations.

In this paper we present observations of organic nitrates obtained during the UBWOS 2012 experiment (15 January–29 February 2012). We further describe the role of organic nitrates in wintertime ozone production and the associated temperature effect by comparing the α values either constrained by observed ΣANs concentration or derived from temperature-dependent yields from VOC composition data. The findings show organic nitrate formation to be one of the primary radical sinks at this site and confirm that the temperature-dependent kinetics are important. However, temperature dependence of organic nitrate yields are not presented in any of the standard photochemical mechanisms used in chemical transport models. Accounting for the temperature dependent yields at 0 °C (the typical daytime temperature during this field campaign) results in a 30 % faster organic nitrate formation rate than what would occur at room temperature (300 K). As a result, we estimate a suppression in OH concentrations by 15 % and ozone formation by 20 % relative to the calculations that do not include the temperature dependence of the $RONO_2$ yields.

2 Instrumentation

The 2012 Uintah Basin Winter Ozone Study occurred from 15 January to the end of February at Horse Pool, Utah, a site approximately 30 miles south of the city of Vernal, Utah. This site was located amid intensive oil and gas extraction operations near the

Discussion Paper | Discussion Paper | Discussion Paper | Discussion Paper |

center of Uintah Basin, with dense gas production wells to the south and oil production wells to the south-west (refer to Fig. 1 of Edwards et al., 2013). A 19 m high tower was on-site for setting up measurements at various heights.

Thermal Dissociation-Laser Induced Fluorescence (TD-LIF) was used to measure NO_2, total peroxy nitrates (ΣPNs = $\Sigma ROONO_2$) and total alkyl nitrates (ΣANs = $\Sigma RONO_2$) using methods described previously. (Day et al., 2002; Thornton et al., 2000) Briefly, laser induced fluorescence was used for detection of gas phase NO_2 using a CW solid-state tunable fiber laser (~ 80 mW, NovaWave) at 530 nm for excitation with detection of photons at wavelengths longer than 700 nm using a red-sensitive PMT (Hamamatsu H7421) preceded by a dielectric long-pass filter. Quartz tubes with external heating elements were maintained at 180 °C for conversion of ΣPNs and 380 °C for ΣANs to NO_2 under a residence time of ~ 20 ms. Simultaneous measurements of NO_2, ΣPNs and ΣANs were achieved by operating 3 LIF cells, each measuring the cumulative concentration of NO_2-yielding compounds.

Corrections are necessary for the TD channel signals. As a negative interference, O_3 pyrolysis and subsequent O atom-initiated chemistry in the TD oven reduces the amount of NO_2 observed for a temperature in excess of 270 °C. This effect is prominent when the contribution of ΣANs is small compared to ambient NO_2. The correction is an empirical relationship developed in the laboratory by directly observing the loss of the 380 °C signal as a function of both O_3 and NO_2 concentrations in the presence of an organic nitrate surrogate (2-ethylhexyl nitrate, Sigma Aldrich). Details of this correction are included in the Appendix A. The factors applied during the daytime hours that are the focus of this study were typically 6–17 % of the total 380 °C signal, of which ΣANs account for approximately 25 %. This amounts to a correction of 24–68 % of the final ΣANs concentration. Larger corrections were required at night due to higher NO_2 concentration. There are also additional contributions from inorganic species, including N_2O_5 (which decomposes to NO_2 and NO_3 at ~ 90 °C) in the 180 °C channel and $ClNO_2$ (which decomposes to a chlorine atom and NO_2, Thaler et al., 2011) in the 380 °C channel. However, accounting for the inorganic signal was straightforward since direct

Discussion Paper | Discussion Paper | Discussion Paper | Discussion Paper |

measurements of both species were available at the site. (Wagner et al., 2011; Roberts et al., 2009) Overall, the $ClNO_2$ contribution to the difference signal between 380 °C and 180 °C was only significant during the night and early morning since, for example, the noontime photolysis lifetime of $ClNO_2$ is only 1 h. We note that N_2O_5, present only during nighttime, did not affect daytime ΣPNs measurements.

In subsequent analyses, ΣPNs is calculated as the difference in concentrations of the ambient and 180 °C channel minus the N_2O_5 contribution, while ΣANs is the concentration difference between the 180 °C channel and the O_3-corrected 380 °C channel minus the $ClNO_2$ contribution.

The TD-LIF instrument was calibrated hourly with a 5 ppm NO_2 gas standard diluted with zero air to generate 5 different concentration levels at the inlet manifold. In addition, the instrument zero (baseline) was monitored every half-hour by overflowing the inlet with NO_x-free zero air. The NO_2 concentration measured by LIF and nearby chemiluminescence instrument were within 7 % of each other on average, giving a linear slope (LIF vs. chemiluminescence) of 0.94, an intercept of 0.02 ppb, and an R^2 value of 0.97.

The inlet was mounted on the southern face of the tower, 16 m above the ground. Other measurements made from similar heights include NO and NO_y (Kliner et al., 1997), speciated VOCs (Goldan et al., 2004), O_3 and photolysis rates for O_3 (O^1D), NO_2 and NO_3. These measurements are described elsewhere (see description and the Supplement Table S1 in Edwards et al., 2013). Temperature, pressure, relative humidity, wind direction and windspeed were measured from the top of the tower. 3-D wind data were measured using the High Resolution Doppler Lidar (Grund et al., 2001) nearby.

3 Results

3.1 Observations

Figure 1 shows the time series (as hourly average) of NO_2, ΣANs, O_3 and windspeed through the observational period. The time-of-day median values of NO_2, ΣANs and O_3 are plotted in Fig. 2. During periods with windspeed lower than 5 m s^{-1}, the chemical species, such as large volatile organic compounds (VOCs) and NO_x, accumulate, leading to an increase in concentrations until high wind episodes occur that flush the basin with clean air. The onset of high wind episodes were therefore coincident with a rapid decrease in VOCs and NO_x concentrations. During the UBWOS campaign in the year before (2011), up to 200 ppb ozone was observed at the end of accumulation periods with snow cover on the ground. However, during similar period in the 2012 campaign, there was little snow and the ozone concentration did not exceed 51 ppb.

3.1.1 NO_2

NO_2 showed a clear diurnal variation (Fig. 2). Concentrations were highest in the early morning when vehicle traffic as well as oil well machinery emissions became coincident with a stable nocturnal boundary layer. Turbulent mixing in the afternoon diluted the concentration, giving a minimum at 4 p.m. local time. The multi-day effect of high/low wind episodes on NO_2 concentration is visible for which high windspeed always corresponds to low NO_2 levels (Fig. 1).

3.1.2 ΣANs

The daily variation in ΣANs concentration is less pronounced than for NO_2 but follows a similar multi-day trend controlled by meteorology. As shown in Fig. 2, the total $RONO_2$ concentration increases in the morning to a noon time peak of 1.5 ppb. The contributions from C_1-C_3 alkyl nitrates measured by GC-MS are small and nearly constant at ~ 50 ppt and did not contribute to the diurnal profile observed.

3.1.3 O_3

The observed O_3 concentration ranged from 4 to 50 ppb and was negatively correlated with NO_2. The diurnal profile has a maximum concentration in the late afternoon, corresponding to a delay of roughly 4 h from the peak of organic nitrates. The increase in O_3 concentration is most rapid (~ 2.4 ppb h^{-1}) at noon.

3.1.4 VOCs

The VOC composition is influenced heavily by the fossil fuel extraction operations. Alkane oxidation dominates the chemistry in the basin (Table 1), accounting for 67 % of total measured VOC reactivity (7.5 s^{-1}) at noon. The diurnal profile of VOCs follows NO_2, reaching a minimum in the late afternoon (see Fig. 3a in Edwards et al., 2012).

3.2 The average branching ratio for nitrate formation

The average noontime temperature during the UBWOS experiment was 0 °C. These cold temperatures provide a unique opportunity to examine the role of temperature on the formation of organic nitrates and the associated radical chain termination compared with other field campaigns taking places in summer.

Organic nitrate compounds are formed via OH-initiated oxidation. For the specific mixture of VOCs observed, the dominant reaction starts with hydrogen abstraction from alkanes by OH. The resulting alkyl radical rapidly reacts with O_2 to give alkyl peroxy radical RO_2, which subsequently reacts with NO to form an energy-rich adduct of the structure $ROONO^*$ (Reaction R1). Under typical atmospheric conditions, a fraction (Reaction R2) of $ROONO^*$ is collisionally stabilized to form the nitrooxy group, $RONO_2$, while the unstabilized portion (Reaction R3) dissociates to yield an alkoxy radical and NO_2. The fate of the alkoxy radical varies depending on the carbon backbone but, in

general, returns a HO_2 radical.

$$RO_2 + NO \rightarrow ROONO^* \quad \text{(R1)}$$

$$\alpha \qquad ROONO^* + M \rightarrow RONO_2 + M \quad \text{(R2)}$$

$$(1-\alpha) \qquad ROONO^* \rightarrow RO + NO_2 \quad \text{(R3)}$$

Given a rate of VOC reaction with OH, the key factor regulating $RONO_2$ production is the nitrate branching ratio, α, defined as the overall fraction of the RO_2 + NO reaction that gives an organic nitrate product rather than an alkoxy radical and NO_2 product. The association reaction to form $RONO_2$ is compound-specific and temperature- and pressure-dependent (Atkinson et al., 1983). In the subsequent sections, we present 2 independent methods for estimating ensemble-averaged α values (or $\langle\alpha\rangle$) for the specific environment of UBWOS campaign, and demonstrate they agree to within the uncertainty of our observations. The first method (Sect. 3.2.1) is based on parameterizations derived from laboratory experiments and the observed VOC composition data, while the second method (Sect. 3.2.2) uses the observed ΣANs concentration, photolysis and VOC reactivity.

3.2.1 VOC-ensemble method

The averaged α, $\langle\alpha\rangle$, is defined in equation below as the summation of compound-specific α values weighted by their relative importance in atmospheric oxidation calculated as the product of OH reaction rate constant and compound concentration (namely, the OH reactivity).

$$\langle\alpha\rangle = \frac{\sum_i k_i[x_i]\alpha_i}{\sum_j k_j[x_j]} \quad (1)$$

Here α_i denotes the compound-specific nitrate branching ratio, k_i (k_j) the OH reaction rate and $[x_i]$ ($[x_j]$) the concentration of species i (j). The VOC OH reactivity, $k_i[x_i]$

($k_j[x_j]$), in the Uintah basin was dominated by alkanes (see Table 1). We point out here that the net effect of temperature on the OH reaction rate constants was generally small, typically a 5 % reduction in total OH reactivity compared with 298 K values (Atkinson, 1994) and the dominant temperature dependence of organic nitrate production is due to the nitrate branching ratio as detailed below.

For α_i specific to alkanes, we use temperature- and pressure-dependent, compound-specific α_i values (Carter and Atkinson, 1989) and include contributions of secondary organic nitrate formation after alkoxy radical isomerization reactions which can be increasingly important for alkanes larger than butane. This increases the individual organic nitrate yield by up to 30 %, generally proportional to the size of the molecule. The compound-specific α values are summarized in Table 2.

The α_i value for aldehydes were treated as having the same nitrate yield as the RO_2 having one less carbon, since the major reaction with OH involves aldehydic hydrogen abstraction and decomposition following reaction with NO to give a CO_2 and a C_{n-1} alkyl radical. α for ketones were estimated using the same method as detailed for alkanes. Methanol and ethanol are presumed to have zero nitrate yield, since their reactions with O_2 after hydrogen abstraction to form carbonyls and HO_2 are dominant. Finally, the nitrate yields for aromatics were set to 1 % in this analysis, following the yield of benzyl nitrate from toluene oxidation (Gery et al., 1985; Atkinson and Aschmann, 1989; Atkinson, 1994). The alkyl nitrate yields from aromatics are likely related to the ring-opening products and are still poorly constrained.

The average nitrate formation yield, $\langle\alpha\rangle$, as calculated above including all VOC and CO measurements throughout the campaign period, is plotted in Fig. 3 as instantaneous values (gold) and as a daytime (08:00 a.m.–06:00 p.m.) average (red filled symbol). The organic nitrate yield ranged from 3 % to 15 % with low values corresponding to periods of high winds (e.g. 3 February). Variation in VOC concentration and composition is the dominant factor controlling the day to day variation as well as the variation over each day. Daytime averaged values of $\langle\alpha\rangle$ calculated at a temperature of 300 K are shown in blue. Even at 300 K the $\langle\alpha\rangle$ is significant, often around 10 %.

3.2.2 Oxidation-production method

Our second approach to estimating α is based primarily on the ΣAN measurements. In this case, $\langle\alpha\rangle$ can be expressed as the ratio of the ΣAN production rate over the total VOC consumption rate (Eq. 2a).

$$\langle\alpha\rangle = \frac{p(\Sigma\mathrm{ANs})}{[\mathrm{OH}]\cdot\sum_i k_i[x_i]} \tag{2a}$$

$$p(\Sigma\mathrm{ANs}) = \frac{\mathrm{d}(\Sigma\mathrm{ANs})}{\mathrm{d}t} + k_{\mathrm{mix}}\cdot\Sigma\mathrm{ANs} \tag{2b}$$

$$[\mathrm{OH}] = f\Big(\sum_i k_i[x_i], J, \langle\alpha'\rangle\Big) \tag{2c}$$

The individual terms in Eq. (2a) can be derived from observations, as shown in Eq. (2b) and (2c). The total production rate of ΣANs ($p(\Sigma\mathrm{ANs})$) is expressed, according to mass balance, as the sum of the rate of change of the observed ΣAN concentration and an overall loss term in Eq. (2b). Chemical losses of ΣANs are found to be negligible compared with turbulent mixing out of the boundary layer. To estimate this effective loss rate constant “k_{mix}”, we employ a tracer method by solving Eq. (2b) using n-propyl nitrate concentrations measured by GC-MS. We chose n-propyl nitrate because its expected loss is also dominated by mixing due to the long chemical lifetime, and its production rate can be calculated independently from measured VOC precursors. Note here that the OH concentration is needed to calculate the production rate of n-propyl nitrate, as well as the VOC consumption rate in the denominator of Eq. (2a). The OH concentration is a function of VOC reactivity and photolysis rates (J values) as well as the α value for the radical recycling efficiency. Due to the dependence of the OH concentration on the nitrate yield, it is not possible to represent α in a closed functional form using all other variables. Therefore, the set of equations must be solved iteratively until a self-consistent α and OH concentration are obtained ($\langle\alpha\rangle = \langle\alpha'\rangle$).

The calculations proceeds as follows by calculating the following: (1) OH concentration and VOC consumption rate, (2) mixing rate estimates, (3) ΣANs formation rate and $\langle\alpha\rangle$.

1. *OH concentration and VOC consumption rate*:

   We used photolysis rates of O_3, NO_2, NO_3, HONO, $ClNO_2$, acetaldehyde, acetone, formaldehyde and HNO_3 to calculate OH and HO_2 production rates. OH formation from alkene ozonolysis reactions was negligible. The medium total radical production of 2.5 ppb day^{-1} is similar to the value reported by Edwards et al. (2013). Data for NO, NO_2 and VOCs coupled with literature values of OH reaction rate constants corrected for campaign measured temperature and pressure dependence (Atkinson et al., 2004, 2006) were then used for OH and HO_2 calculations including radical recycling. The resulting VOC consumption rate is shown in Fig. 4. Note the VOC consumption rate profile conforms more to the shape of the radical source strength (OH and HO_2 formation rate derived from photolysis, same shape as solar irradiation) than to the OH concentration, consistent with the notion that VOCs are the major reaction partner with OH.

2. *Mixing rate estimation*:

   We estimate the dilution loss (k_{mix}) for ΣANs concentration by substituting [ΣANs] with n-propyl nitrate concentration in Eq. (2b). The time derivative of n-propyl nitrate concentration was calculated using a finite difference method, followed by application of a 2 h running mean to smooth hourly data. Kinetic studies dictate that ∼ 24 % of the OH reaction with propane at 273 K yielded a primary alkyl radical, (Droege and Tully, 1986) which promptly reacted with O_2 to form the corresponding peroxy radical. Larger alkane molecules can also yield n-propyl alkyl radical as a result of alkoxy radical decomposition from the appropriate structure, and we accounted for all such minor formation channels up to undecane to give a total additional contribution of 14 % from sources other than propane. The total formation rate of n-propyl nitrate is presented in Fig. 4 as the red trace spanned

   by the 25 and 75 percentiles in the shaded area. Plotted in blue is the median value of time derivative of n-propyl nitrate concentration showing a diurnal pattern for which peak concentration was reached at noon time when the time derivative crosses the zero line. The initial concentration increase roughly coincides with the start of photochemical reaction, as is also marked by the onset of n-propyl nitrate formation rate. The negative portion of the blue trace in the afternoon then corresponds to faster dilution due both to turbulence and to the elevated concentration. These values are sufficient to solve for the time-varying dilution rate constant, k_{mix}, shown in Fig. 5 as green line with dashed traces bounding the interquartile range. Note the slight delay (∼ 1 h) in the daily maximum of the dilution rate constant when compared with the peak of n-propyl nitrate formation rate. As vertical turbulence was promoted by surface heating, this delay is a reasonable consequence of the expected lag in the mixing rate. The median daily maximum mixing rate shows a time constant of 6 h, much more rapid than other loss processes such as the OH oxidative lifetime of n-propyl nitrate of over 150 h under the OH concentration of 2×10^6 cm^{-3} (Fig. 4) and a photolysis lifetime of over 200 h, (Luke et al., 1989) consistent with our initial assumption that chemical losses are small.

3. *ΣANs formation rate and* $\langle\alpha\rangle$:

   Using the k_{mix} calculated above, the ΣAN formation rate was estimated using Eq. (2b). We then inserted this ΣAN formation rate and VOC consumption rate back into Eq. (2a) to obtain the implied $\langle\alpha\rangle$ value based on the field observations and also the initial guess of $\langle\alpha'\rangle$. For time periods when $\langle\alpha\rangle$ mismatches $\langle\alpha'\rangle$, $\langle\alpha'\rangle$ is adjusted toward $\langle\alpha\rangle$ accordingly and the calculation repeated to achieve consistency. To reduce the number of points needed for calculation, we only estimated one self-consistent $\langle\alpha\rangle$ value for each day by averaging from 8 a.m. to 6 p.m., the same as the averaging window used for our first method.

   Direct comparison of the estimate from Sect. 3.2.2 with the one derived from just the VOC composition (Sect. 3.2.1) is shown in Fig. 6. There were 27 days to compare and the two methods are nearly identical, yielding a slope of 1.06 and $R^2 = 0.61$. The similarity in results of the two methods lends support to the estimates of α and confirms the importance of a significant temperature dependence to the value of α affecting the UBWOS chemistry.

4 Discussion

The relatively high value observed for the average nitrate yield, $\langle\alpha\rangle$, of ~ 15 %, is a direct consequence of low temperatures and the presence of heavy alkanes, a special condition created by natural gas and oil extraction operations in the basin. In the following sections, we discuss how this elevated nitrate yield affects the fate of NO_x emitted into the basin and the rate of local O_3 production.

4.1 Fate of NO_x

Organic nitrate formation was a significant chemical loss for NO_x in the Uintah Basin. We calculated that alkyl nitrate formation is 50 % faster than HNO_3 formation during the low wind periods, of 0.23 ppb h^{-1} vs. 0.16 ppb h^{-1} using the estimated noontime OH concentration. Together, this amounts to a NO_x chemical lifetime of 17 h, with relative branching of 59 % to alkyl nitrate formation and 41 % to HNO_3 formation. PAN and other peroxyacyl nitrate compounds were not observed to have high production rates based on measured ΣPNs and PAN concentration and direct calculation of their formation rate from VOC composition including aldehydes. We estimate a lower and upper limit in noontime median net production of 0.01 to 0.06 ppb PAN h^{-1}, using bottom-up (VOC speciation) and top-down (observed PAN concentration and dilution rate assuming zero background PAN concentration) methods, respectively. This corresponds to PAN representing a maximum of ~ 18 % of the NO_x sink. Alkyl nitrate formation is therefore the single most important chemical loss pathway for NO_x as well as the most important terminator for OH chain propagation. Note that, although ΣAN formation is

the largest chemical sink, mixing out of the basin is the dominant overall loss for NO_x emitted. We estimate 68 % of NO_x loss is to transport out of the basin.

4.2 O_3 formation

O_3 formation is closely related to the formation of organic nitrates, since the reaction channels lead from a branching point in a common pathway. Similar to our treatment of VOC-specific α values, we calculated, for each measured VOC molecule, the average number of O_3 molecules generated in a single event of OH initiated oxidation, denoted as γ in Table 2. Note that our definition and estimate for γ includes the contribution from multi-generation alkyl nitrate formation, making it slightly different from previous calculations (Rosen et al., 2004; Perring et al., 2013; Farmer et al., 2011) (see Appendix C). The O_3 production rate is then a product of the ensemble-averaged γ and the VOC consumption rate calculated above, as plotted in Fig. 7. The difference between the O_3 production rate and the rate of change in O_3 concentration signifies the contribution of mixing into the background air. When compared with the production characteristics of n-propyl nitrate in Fig. 4, it is apparent that dilution loss is much more important for the case of n-propyl nitrate (> 80 % of the formation rate) than for O_3 (~ 30 % of formation rate). Using the k_{mix} derived from n-propyl nitrate formation, the local O_3 budget of the whole campaign period can be closed with a background O_3 concentration in the range of 20–35 ppb, consistent with observations during high wind periods. This also reinforces the notion that our estimate for turbulent mixing is representative. To reproduce the short-term variations in O_3 production over a 72 h period with a fixed background O_3 level of 30 ppb, we estimate the expected change in O_x (O_3+ NO_2) concentration using the mass balance equation (Eq. 2b) to find reasonable agreement with the observations (Fig. 8).

Regarding the relative production of O_3 to ΣANs, the average $p(O_3)/p(\Sigma\text{ANs})$ calculated as γ/α for UBWOS is 15. For comparison, a value of 6.2–7.5 was reported for the Deep Water Horizon (DWH) plume study (Neuman et al., 2012). While both plumes were dominated by alkanes, the VOC suite for the DWH study was further enriched in heavier organics. By comparison, a typical industrial city plume (Rosen et al., 2004) measured around Houston during Texas Air Quality Study 2000 has a value of 29–41, a direct result from low α value (6.5–4.7 %) caused by high temperature (~ 40 °C) and relatively low contribution from large alkanes.

4.3 Temperature

Currently, none of the chemical mechanisms commonly employed in the chemical transport models for regional O_3 predictions have incorporated the temperature dependence of alkyl nitrate yields. Since alkyl nitrate formation is a radical termination reaction, reduction in temperature decreases the OH recycling probability and shortens the OH radical chain length. For the 2012 UBWOS campaign the effect is to reduce the radical propagation chain length from a noontime median of 3.2 (300 K) to 2.6 (273 K). Since the chain length is directly proportional to the O_3 production rate, this corresponds to a 20 % decrease in the O_3 formation rate. Table 3 shows the estimated maximum O_x concentration in a multi-day low wind accumulation event in the Uintah Basin based on the observed alkyl nitrate yield. We compare a calculation at 300 K to one at 273 K. Note that for a snowless winter condition, such as encountered in UBWOS 2012, the prediction matches well with the observed maximum hourly O_x concentration of 51 ppb in the afternoon of 18 February 2012. While estimating the α value at 300 K always yields a higher predicted O_3 concentration, the over prediction is greatest for the simulated snow condition (right most column) when persistent snow cover increases the photolysis rate and stabilizes the boundary layer impeding mixing.

5 Conclusion

We presented an analysis of field observations obtained in the Uintah Basin during winter 2012 in Utah, USA. We find that the field data can be used to derive the temperature dependence of the ensemble-averaged nitrate yield, $\langle\alpha\rangle$, and that this value

is consistent with a parameterization derived from laboratory experiments. Including the proper temperature dependence based on the dominating VOC species should be considered for models aimed at estimating local O_3 concentrations in order to avoid substantial errors (+15 % at 0 °C from 27 °C values).

Appendix A: O_3 pyrolysis correction for ΣANs (380 °C) channel

It was necessary to correct for apparent negative signals observed in the ΣANs signal (ΣANs channel showing less signal level than the ΣPNs channel). The cause of this interference was O_3 pyrolysis to yield O atom in the TD oven at elevated temperature. In the absence of organic molecules, the O atom can serve as a promoter for NO and NO_2 interconversion reaction, as illustrated in Reactions (R4)–(R7).

$$O_3 + M \rightarrow O_2 + O + M \tag{R4}$$

$$O_2 + O + M \rightarrow O_3 + M \tag{R5}$$

$$NO_2 + O \rightarrow NO + O_2 \tag{R6}$$

$$NO + O + M \rightarrow NO_2 + M \tag{R7}$$

NO and NO_2 are interconverted at a cost of one O atom whose steady state concentration is generally controlled by the forward and reverse Reactions (R4) and (R5). If sufficient time is given, NO and NO_2 will ultimately reach an equilibrium ratio which can be calculated from the reaction rate $k_{1.2}$ and $k_{1.3}$ (of Reactions R5 and R6, respectively) with pressure dependence. From the O_3 pyrolysis rate and the gas residence time of 0.17 s in our TD oven region, only ΣANs channel at 380 °C should generate sufficient O atom to significantly alter the NO_2 concentration. To confirm this effect, we performed a series of lab experiments under NO_x and O_3 concentrations covering the range observed during the UBWOS campaign in the presence of ~ 2 ppb of 2-ethylhexyl nitrate, a simple alkyl nitrate standard available from Sigma Aldrich as a surrogate for the collection of ΣANs in Utah. Figure A1 demonstrates the result from a temperature scan experiment when the inlet oven temperature of cell 1 was scanned upward from 180 °C to 380 °C, the operating temperature of ΣANs channel in the field. The red trace represents the NO_2 signal from cell 1, while the black trace is the NO_2 signal from cell 3 whose inlet was unheated. Since there was no peroxy nitrate in the system, at 180 °C cell 3 only detect the same amount of NO_2 as the ambient temperature cell 1. However, starting from ~ 200 °C alkyl nitrate started to thermal dissociate, giving extra NO_2 signal as the red trace increased relative to the black trace. At temperature beyond 280 °C effects due to O_3 pyrolysis started to reduce the excess NO_2 signal, presumably by the interconversion reaction mentioned above and we see the red trace eventually dropped below the black trace at around 320 °C. This interference thus generated substantial negative ΣANs signal when we subtract the 180 °C channel from 380 °C channel. Indeed, significant portions of uncorrected night time ΣANs signals throughout the campaign yielded negative values including negative spikes correlated with positive NO_2 spikes from nearby road traffic emissions. This effect was most prominent when high NO_2 concentration existed so that the excess ΣANs signal was relatively small on the 380 °C channel. Considering that under the same O_3 concentration the fraction of NO_2 converted due to O atom chemistry was a constant, larger overall NO_2 concentration corresponded to a larger overall NO_2 reduction which could easily overwhelm the original ΣANs signal to introduce negative values when high temperature channel was subtracted from lower temperature ones. For example, we have performed high temperature box model simulations on O_3 pyrolysis reactions inside the TD oven with a residence time of 0.17 s. At an O_3 concentration of 30 ppb the amount of NO_2 loss through 380 °C was around 6 %. This indicates that if the ΣANs fraction within a sample is less than 6 % of the total concentration from NO_2, ΣPNs and ΣANs combined, a negative value will result. The O atom chemistry outlined in Reactions (R4)–(R7) was further complicated by the presence of organics, especially when initial NO_2 concentration was small as signal loss in lab experiments was always more than can be explained in the absence of organics. Since we were uncertain of the effect of possible chain reactions involving organic radicals initiated by O atom, an empirical

equation derived directly from in-lab observations under NO_x and O_3 concentrations relevant to UBWOS condition was currently used for such correction. Equation (A1) shows the relation of fractional signal lost (r) as a function of the observed total signal S_{380} of the 380 °C channel ($NO_2 + \Sigma PNs + \Sigma ANs$) and O_3 concentration with all parameters obtained through fitting of experimental data. The corrected signal (S'_{380}) was thus obtained with Eq. (A2).

$$r = (0.0694 \times \ln(S_{380}) - 0.308) \times (0.0115 \times [O_3] + 0.557) \tag{A1}$$

$$S'_{380} = \frac{S_{380}}{1 + r} \tag{A2}$$

Appendix B: VOC α calculation considering multiple generation RO_2 formation

Explicit examples for calculating α are given in the following sections for OH-initiated oxidation of ethane and propane in the presence of NO. Further generalizations to other organics are also described.

B1 α for ethane

Estimating α for ethane is relatively straightforward. Daytime oxidation of ethane starts with an initial hydrogen extraction by OH radical followed by O_2 addition to the alkyl radical formed. Only a single isomer of alkyl peroxy radical is involved and no significant decomposition channel exists for the ethyl alkoxy radical formed from NO reaction that does not yield organic nitrate, as shown in Fig. B1. We simply state here and will demonstrate in later section that the dominant fate of RO_2 radicals in the basin were reaction with NO because RO_2-RO_2 and RO_2-HO_2 reactions are minor during the day. The number in bracket is specific branching ratio of the processes represented. Branching ratios yielding organic nitrates are colored in blue. The overall nitrate branching ratio in this simple case is the same as the specific branching ratio of the ethylperoxy radical at 0.019.

B2 α for propane

To calculate the overall nitrate yield for propane, the dominant product channels should be traced, as illustrated in Fig. B2. Two isomers are formed through hydrogen extractions from either the primary or secondary carbon, giving n-propylperoxy and isopropylperoxy radical in a relative yield of 24 % and 76 %, respectively. The overall nitrate branching ratio can then be calculated if the specific α for each peroxy isomer is known. Starting from n-propylperoxy radical, the direct reaction with NO gives n-propyl nitrate with a relative yield of 2.1 % calculated according to the Carter and Atkinson's method at 273 K and 842 mBar, representative of campaign condition. The remaining portion of the channel proceeding through alkoxy radical reactions has a further branching of decomposition reaction (rather than reacting with O_2) to form a formaldehyde and an ethyl radical which promptly reacts with O_2 to give ethylperoxy radical. The relative yield of decomposition vs. O_2 reaction can be calculated from the respective reaction rates reported in the literature. We used a decomposition rate of $846\,s^{-1}$ (Curran, 2006) and the product of O_2 reaction rate with O_2 concentration giving a first-order rate constant of $4 \times 10^4\,s^{-1}$ for the O_2 channel. Branching ratios are hence 2 % and 98 % for decomposition and O_2 reaction. The ethylperoxy radical from the decomposition channel can then react further with NO to give organic nitrates with a yield of 0.019, calculated in the previous section. Summing up both yields scaled by the individual channel strength, we have the specific nitrate yield of n-propylperoxy radical as: $(0.019 \times 0.02 \times 0.979 + 0.021) = 0.021_4$. Note the correction from the additional ethylperoxy radical nitrate yield is almost negligible, due to the decomposition channel strength of only 2 %. However, for larger molecules, typically starting from n-butane, isomerization reactions can contribute substantially and higher-generation nitrate yield corrections are generally non-negligible. For iso-propylperoxy radical the specific nitrate yield was calculated using the same principle, only that after decomposition reaction a methylperoxy radical is formed. Since methylperoxy radical has little yield for methylnitrate formation, the total specific nitrate yield for iso-propylperoxy radical is just the direct yield of 5.2 %. The overall α for propane-OH reaction is hence the ensemble average of the specific nitrate yield of all peroxy isomers, namely: $(0.24 \times 0.021 + 0.76 \times 0.052) = 0.045$.

B3 α for higher alkanes and other organics

Using the method detailed above for propane, we carried out an extended estimation for alkanes up to undecane which is the largest alkane reported from GC-MS data. The results are summarized in Table 2. It is noted here that certain simplifications were necessary for this calculation. For example, in estimating α for more complex RO_2 radicals from higher-generation oxidation products we ignored the possible contribution of other oxygen-containing functional groups toward the estimated yield given by the Carter and Atkinson parameterization so that only carbon number was considered. Further, rate constants used to estimate the relative branching ratios of alkoxy radical reactions were limited to available literature values, generally around 298 K. As carbon chain length becomes longer, experimental data regarding O_2 reaction, isomerization and decomposition rates become scarce and the data available for the most similar structure are used.

Appendix C: Differences in definition of γ used in this work

The γ value, used to denote the amount of O_3 molecule generated from OH-initiated oxidation of an organic molecule in this work, is different from the definition of previous works that focus on only single generation RO_2 chemistry in 2 respects, described as following. First, γ has commonly been given a value of 2 for two O_3 molecules being generated per OH-initiated oxidation of VOCs, from the formation of HO_2 and NO_2 each. This is a good approximation for small alkanes of which isomerization is not important, but can be erroneous otherwise. For example, in the absence of organic nitrate formation channel, we estimate γ for n-hexane to be 3.2 due to the efficient isomerization reaction of hydrogen abstraction by the 2-alkoxy or 3-alkoxy radical produced, generating a new alkyl radical and an alcohol group. The presence of large alkanes, up to undecane, necessitates a more careful treatment. Second, γ has been used to calculate the ratio of O_3 production rate over ΣANs production rate, formulated as $\gamma(1-\alpha)/\alpha$. The factor $(1-\alpha)$ in the numerator implies that γ was estimated under the assumption of zero nitrate formation. $(1-\alpha)$ therefore accounted for the fraction of reaction that actually proceeded to form O_3. This is only exact if VOC + OH reaction only forms a single generation of RO_2 molecule, once again a valid assumption for small VOC only. For larger alkanes there exist a non-negligible fraction of higher generation RO_2 reactions from isomerization reactions and we must account for the effective number of NO_2 and HO_2 formed in a cumulative manner over extended generations. This means γ and α are related by the structure of the molecule under consideration. Our listed γ values in Table 2 is then the better average number of O_3 generated per OH-initiated oxidation with alkyl nitrate formation considered, or in the same spirit, the "$\gamma(1-\alpha)$" value considered over multi-generation reactions. In Table 2, we observe an increasing trend of γ going from methane to around hexane as larger alkanes are more susceptible to isomerization and further radical reactions, converting more NO to NO_2. This trend does not continue, however, with further increase of alkane size because of the competing effect of increasing organic nitrate yield, eventually reduces the amount of alkoxy radical formed.

Acknowledgements. The authors acknowledge the NOAA office of global programs: NA13OAR4310067 and NSF AGS-1120076 for their support of this research. The authors also acknowledge Jim Roberts for his hospitality and support in PAN, HONO and $ClNO_2$ data, and Brian Lerner for VOC data.

References

Atkinson, R.: Gas-phase tropospheric chemistry of organic-compounds, J. Phys. Chem. Ref. Data, ISBN: 156396340X, 1994.

Atkinson, R. and Aschmann, S. M.: Rate constants for the gas-phase reactions of the OH radical with a series of aromatic-hydrocarbons at 296 ± 2 K, Int. J. Chem. Kinet., 21, 355–365, doi:10.1002/kin.550210506, 1989.

Atkinson, R., Carter, W. P. L., and Winer, A. M.: Effects of temperature and pressure on alkyl nitrate yields in the NO_x photooxidations of normal-pentane and normal-heptane, J. Phys. Chem., 87, 2012–2018, doi:10.1021/j100234a034, 1983.

Atkinson, R., Baulch, D. L., Cox, R. A., Crowley, J. N., Hampson, R. F., Hynes, R. G., Jenkin, M. E., Rossi, M. J., and Troe, J.: Evaluated kinetic and photochemical data for atmospheric chemistry: Volume I - gas phase reactions of O_x, HO_x, NO_x and SO_x species, Atmos. Chem. Phys., 4, 1461–1738, doi:10.5194/acp-4-1461-2004, 2004.

Atkinson, R., Baulch, D. L., Cox, R. A., Crowley, J. N., Hampson, R. F., Hynes, R. G., Jenkin, M. E., Rossi, M. J., Troe, J., and IUPAC Subcommittee: Evaluated kinetic and photochemical data for atmospheric chemistry: Volume II – gas phase reactions of organic species, Atmos. Chem. Phys., 6, 3625–4055, doi:10.5194/acp-6-3625-2006, 2006.

Carter, W. P. L. and Atkinson, R.: Alkyl nitrate formation from the atmospheric photooxidation of alkanes – a revised estimation method, J. Atmos. Chem., 8, 165–173, doi:10.1007/bf00053721, 1989.

Curran, H. J.: Rate constant estimation for C_1 to C_4 alkyl and alkoxyl radical decomposition, Int. J. Chem. Kinet., 38, 250–275, doi:10.1002/kin.20153, 2006.

Day, D. A., Wooldridge, P. J., Dillon, M. B., Thornton, J. A., and Cohen, R. C.: A thermal dissociation laser-induced fluorescence instrument for in situ detection of NO_2, peroxy nitrates, alkyl nitrates, and HNO_3, J. Geophys. Res.-Atmos., 107, ACH 4-1–ACH 4-14, doi:10.1029/2001jd000779, 2002.

Droege, A. T. and Tully, F. P.: Hydrogen-atom abstraction from alkanes by OH. 3. Propane, J. Phys. Chem., 90, 1949–1954, doi:10.1021/j100400a042, 1986.

Edwards, P. M., Young, C. J., Aikin, K., deGouw, J., Dubé, W. P., Geiger, F., Gilman, J., Helmig, D., Holloway, J. S., Kercher, J., Lerner, B., Martin, R., McLaren, R., Parrish, D. D., Peischl, J., Roberts, J. M., Ryerson, T. B., Thornton, J., Warneke, C., Williams, E. J., and Brown, S. S.: Ozone photochemistry in an oil and natural gas extraction region during winter: simulations of a snow-free season in the Uintah Basin, Utah, Atmos. Chem. Phys., 13, 8955–8971, doi:10.5194/acp-13-8955-2013, 2013.

Farmer, D. K., Perring, A. E., Wooldridge, P. J., Blake, D. R., Baker, A., Meinardi, S., Huey, L. G., Tanner, D., Vargas, O., and Cohen, R. C.: Impact of organic nitrates on urban ozone production, Atmos. Chem. Phys., 11, 4085–4094, doi:10.5194/acp-11-4085-2011, 2011.

Gery, M. W., Fox, D. L., Jeffries, H. E., Stockburger, L., and Weathers, W. S.: A continuous stirred tank reactor investigation of the gas-phase reaction of hydroxyl radicals and toluene, Int. J. Chem. Kinet., 17, 931–955, doi:10.1002/kin.550170903, 1985.

Goldan, P. D., Kuster, W. C., Williams, E., Murphy, P. C., Fehsenfeld, F. C., and Meagher, J.: Nonmethane hydrocarbon and oxy hydrocarbon measurements during the 2002 New England Air Quality Study, J. Geophys. Res.-Atmos., 109, D21309, doi:10.1029/2003jd004455, 2004.

Grund, C. J., Banta, R. M., George, J. L., Howell, J. N., Post, M. J., Richter, R. A., and Weickmann, A. M.: High-resolution Doppler lidar for boundary layer and cloud research, J. Atmos. Ocean. Tech., 18, 376–393, doi:10.1175/1520-0426(2001)018<0376:hrdlfb>2.0.co;2, 2001.

Kliner, D. A. V., Daube, B. C., Burley, J. D., and Wofsy, S. C.: Laboratory investigation of the catalytic reduction technique for measurement of atmospheric NO_y, J. Geophys. Res.-Atmos., 102, 10759–10776, doi:10.1029/96jd03816, 1997.

Luke, W. T., Dickerson, R. R., and Nunnermacker, L. J.: Direct measurements of the photolysis rate coefficients and Henry law constants of several alkyl nitrates, J. Geophys. Res.-Atmos., 94, 14905–14921, doi:10.1029/JD094iD12p14905, 1989.

Neuman, J. A., Aikin, K. C., Atlas, E. L., Blake, D. R., Holloway, J. S., Meinardi, S., Nowak, J. B., Parrish, D. D., Peischl, J., Perring, A. E., Pollack, I. B., Roberts, J. M., Ryerson, T. B., and Trainer, M.: Ozone and alkyl nitrate formation from the Deepwater Horizon oil spill atmospheric emissions, J. Geophys. Res.-Atmos., 117, D09305, doi:10.1029/2011jd017150, 2012.

Perring, A. E., Bertram, T. H., Wooldridge, P. J., Fried, A., Heikes, B. G., Dibb, J., Crounse, J. D., Wennberg, P. O., Blake, N. J., Blake, D. R., Brune, W. H., Singh, H. B., and Cohen, R. C.: Airborne observations of total $RONO_2$: new constraints on the yield and lifetime of isoprene nitrates, Atmos. Chem. Phys., 9, 1451–1463, doi:10.5194/acp-9-1451-2009, 2009.

Perring, A. E., Bertram, T. H., Farmer, D. K., Wooldridge, P. J., Dibb, J., Blake, N. J., Blake, D. R., Singh, H. B., Fuelberg, H., Diskin, G., Sachse, G., and Cohen, R. C.: The production and

persistence of $\Sigma RONO_2$ in the Mexico City plume, Atmos. Chem. Phys., 10, 7215–7229, doi:10.5194/acp-10-7215-2010, 2010.

Perring, A. E., Pusede, S. E., and Cohen, R. C.: An observational perspective on the atmospheric impacts of alkyl and multifunctional nitrates on ozone and secondary organic aerosol, Chem. Rev., 113, 5848–5870, doi:10.1021/cr300520x, 2013.

Roberts, J. M., Osthoff, H. D., Brown, S. S., Ravishankara, A. R., Coffman, D., Quinn, P., and Bates, T.: Laboratory studies of products of N_2O_5 uptake on Cl^- containing substrates, Geophys. Res. Lett., 36, L20808, doi:10.1029/2009gl040448, 2009.

Rosen, R. S., Wood, E. C., Wooldridge, P. J., Thornton, J. A., Day, D. A., Kuster, W., Williams, E. J., Jobson, B. T., and Cohen, R. C.: Observations of total alkyl nitrates during Texas Air Quality Study 2000: implications for O_3 and alkyl nitrate photochemistry, J. Geophys. Res., 109, D07303, doi:10.1029/2003jd004227, 2004.

Schnell, R. C., Oltmans, S. J., Neely, R. R., Endres, M. S., Molenar, J. V., and White, A. B.: Rapid photochemical production of ozone at high concentrations in a rural site during winter, Nat. Geosci., 2, 120–122, doi:10.1038/ngeo415, 2009.

Thaler, R. D., Mielke, L. H., and Osthoff, H. D.: Quantification of nitryl chloride at part per trillion mixing ratios by thermal dissociation cavity ring-down spectroscopy, Anal. Chem., 83, 2761–2766, doi:10.1021/ac200055z, 2011.

Thornton, J. A., Wooldridge, P. J., and Cohen, R. C.: Atmospheric NO_2: in situ laser-induced fluorescence detection at parts per trillion mixing ratios, Anal. Chem., 72, 528–539, doi:10.1021/ac9908905, 2000.

Wagner, N. L., Dubé, W. P., Washenfelder, R. A., Young, C. J., Pollack, I. B., Ryerson, T. B., and Brown, S. S.: Diode laser-based cavity ring-down instrument for NO_3, N_2O_5, NO, NO_2 and O_3 from aircraft, Atmos. Meas. Tech., 4, 1227–1240, doi:10.5194/amt-4-1227-2011, 2011.

Table 1. Median OH reactivity and associated formation rates at local noon.

Compound Class	OH Reactivity (s^{-1})	$p(\Sigma\mathrm{ANs})^*$ ($\mathrm{ppt\,h^{-1}}$)	$p(O_3)^*$ ($\mathrm{ppt\,h^{-1}}$)
Alkane C_1–C_{11}	5.02	172	1760
Alkene C_2-C_3	0.15	0.71	44
Alkyne C_2	0.013	0	2.4
Aromatic C_6–C_9	0.58	0.90	120
Alcohol C_1–C_2	0.31	0	48
Ketone C_3–C_4	0.0084	~ 0	0.37
Aldehyde C_1–C_4	0.44	0	130
CO	0.95	0	150
NO	0.61	0	0
NO_2	0.82	0	0
Total	8.90	174	2250

* Median noon time [OH] = 1×10^6 molecule $\mathrm{cm^{-3}}$.

Table 2. Summary of specific organic nitrate and ozone yield calculated at 0 °C.

Compound Class	α	γ	Compound Class	α	γ
Alkane	**0.22**	**2.25**	**Alkene**	**0.031**	**1.94**
methane	~ 0	2	ethene	0.025	1.95
ethane	0.019	1.96	propene	0.05	1.9
propane	0.045	1.92			
iso-butane	0.11	2.6	**Alkyne**	**0**	**1.2**
n-butane	0.114	2.17	ethyne	~ 0	1.2
iso-pentane	0.21	2.46			
n-pentane	0.2	2.19	**Aromatic**	**0.01**[a]	**1.3**[b]
2,2-dimethylpropane	0.25	3.1			
n-hexane	0.42	2.62	**Alcohol**	**0**	**1**
2,2-dimethylbutane	0.36	2.7	methanol	~ 0	1
2-methylpentane	0.29	2.2	ethanol	~ 0	1.05
3-methylpentane	0.33	2.34			
methyl-cyclopentane	0.29	2.9	**Ketone**	**0.077**	**3.72**
Cyclohexane	0.33	2	acetone	0.021	4
methyl-cyclohexane	0.58	2.4	methylethylketone	0.11	3.56
ethyl-cyclohexane	0.5	2.25			
dimethyl-cyclohexane	0.67	1.8	**Aldehyde**	**0**	**1.96**
heptane	0.6	2.2	formaldehyde	0	1
octane	0.6	1.86	acetaldehyde	0	3
nonane	0.62	1.52	propanal	0.019	3
decane	0.74	1.43	butanal	0.045	2.91
undecane	0.81	1.2	methacrolein	0.05	2.45

[a] Previously assumed value of 0.1 is due to contribution of nitrobenzene which we do not detect in ΣANs channel.

[b] Assumption based on toluene data.

Table 3. Expected maximum O_x ($NO_2 + O_3$) concentration under UBWOS condition.

Condition[a]	UBWOS 2012 base condition	photolysis × 2 and mixing ÷ 2
α calculated at 273 K[b]	57 ppb	140 ppb
α calculated at 300 K[b]	64 ppb	165 ppb
error	7 ppb	25 ppb

[a] Assuming background O_3 concentration of 30 ppb.

[b] Carter and Atkinson (1989).

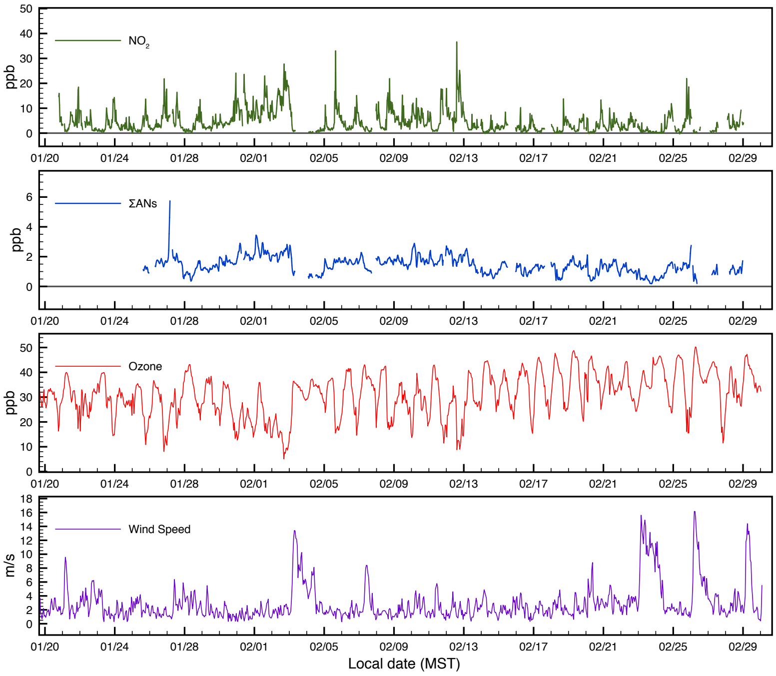

Figure 1. Hourly-averaged time series of NO_2, total alkyl nitrates (ΣANs), O_3 and windspeed measured during UBWOS 2012. The concentrations are measured at height of 16 m from a 19 m scaffolding tower on site. The windspeed is measured at the tower top. Ticks on the x-axis mark local midnight.

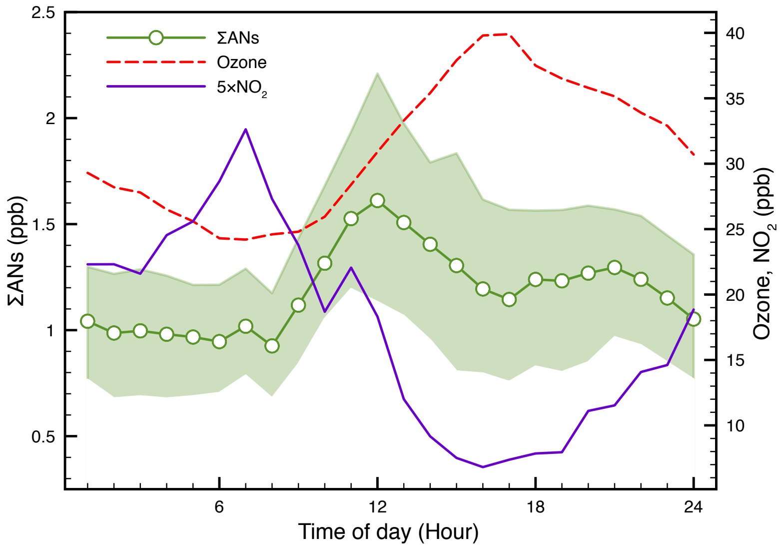

Figure 2. Diurnal variations of ΣANs, ozone and NO_2. Lines represent median values while the shaded area of ΣANs represents the interquartile (25–75 %) coverage. The ΣAN data have been corrected for O_3 and $ClNO_2$ interferences (see text).

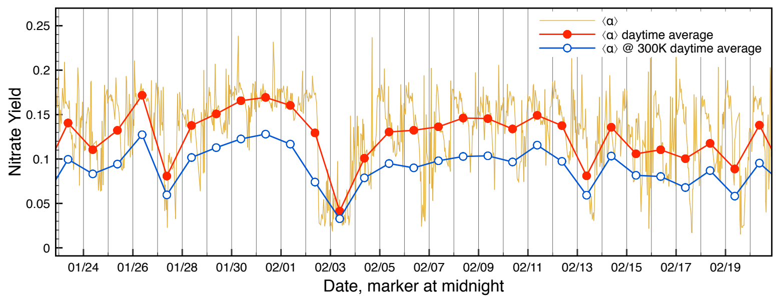

Figure 3. Ensemble-averaged nitrate formation yield ($\langle\alpha\rangle$) calculated based on the method in Sect. 3.2.1. Red symbols represent daytime average of the hourly $\langle\alpha\rangle$ (in orange) estimated at 273 K, representative of the campaign period conditions. The blue symbols are the daytime averaged $\langle\alpha\rangle$ estimated at 300 K, routinely used in global models.

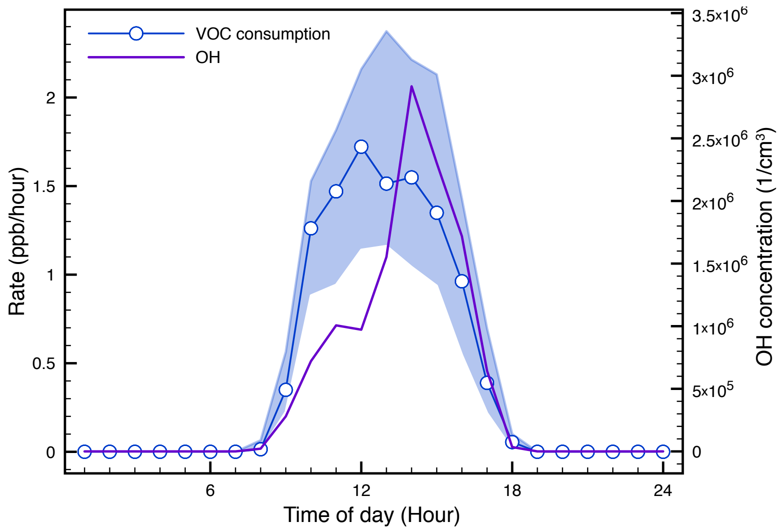

Figure 4. Calculated daytime median profiles of the VOC consumption rate and the OH concentration. The VOC consumption rate is controlled by the photolysis rate leading to OH and HO_2 radical formation, while OH concentration is regulated by the OH reactivity dominated by the NO_x and VOC concentrations.

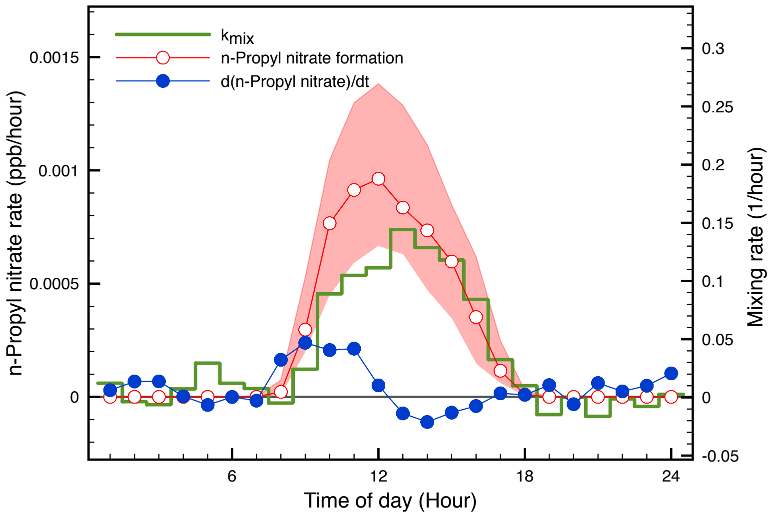

Figure 5. The production rate and concentration change of n-propyl nitrate calculated from field observations. The difference between the red and blue traces represent the mixing loss promoted by solar surface heating. The green trace is the calculated effective first order mixing rate, k_{mix}.

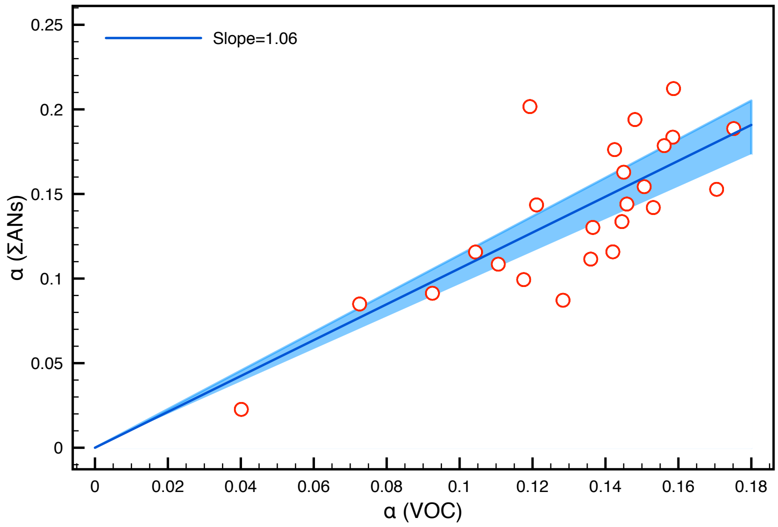

Figure 6. Correlation between daytime averaged *α* estimated using the VOC-ensemble method (VOC, Sect. 3.2.1) and oxidation-production method (ΣANs, Sect. 3.2.2). The shaded area corresponds to the 95 % confidence interval for the regression slope passing through origin. The 1 : 1 line is within this interval.

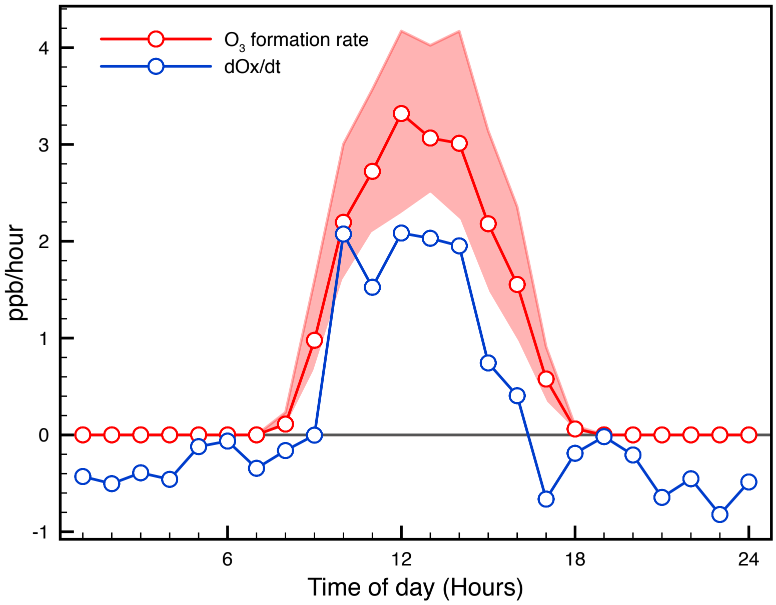

Figure 7. Calculated daytime O_3 formation rate and the rate of change of O_x ($NO_2 + O_3$) observed. The difference between traces can be attributed to mixing using the same mixing rate estimated from n-propyl nitrate. The existence of non-negligible background O_3 concentration (30 ppb) suppresses the net dilution.

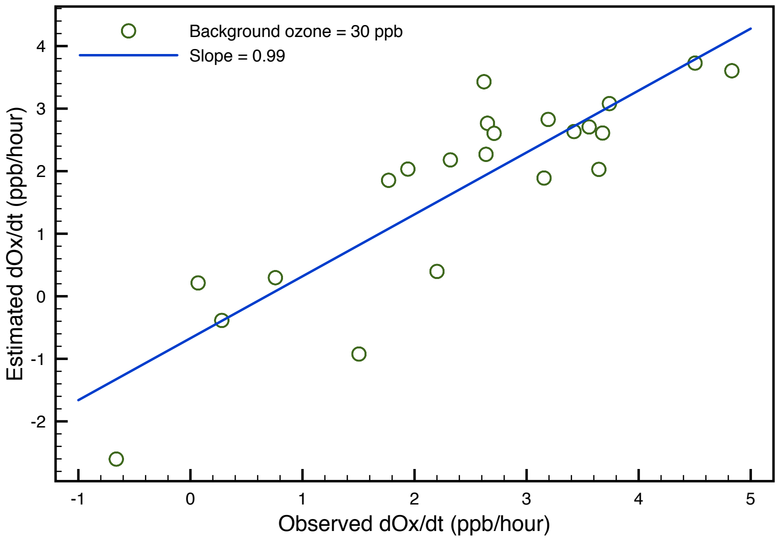

Figure 8. Correlation of the estimated daytime hourly O_3 production rate corrected for dilution loss to what was observed from O_3 and NO_2 data. A background O_3 concentration of 30 ppb was assumed.

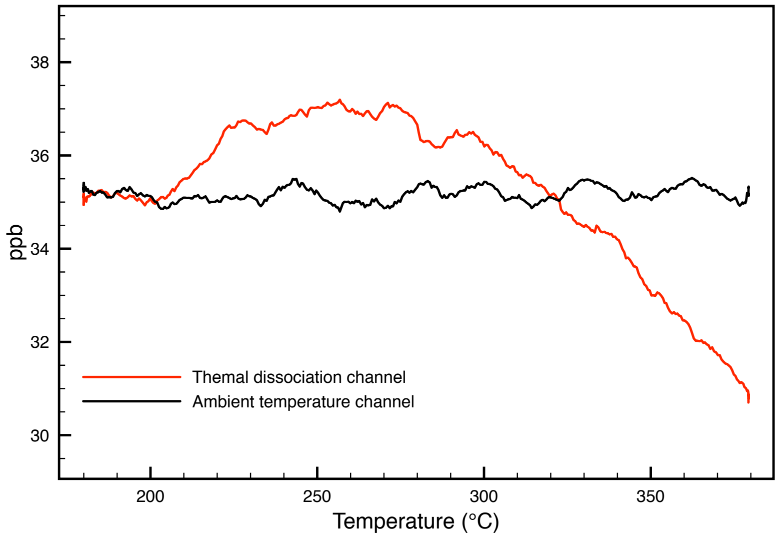

Figure A1. Laser induced fluorescence signal from samples containing ~ 35 ppb NO_2 and 2 ppb 2-ethylhexyl nitrate passing through the unheated channel (ambient temperature, black trace) and thermal dissociation channel (red trace) in the presence of O_3.

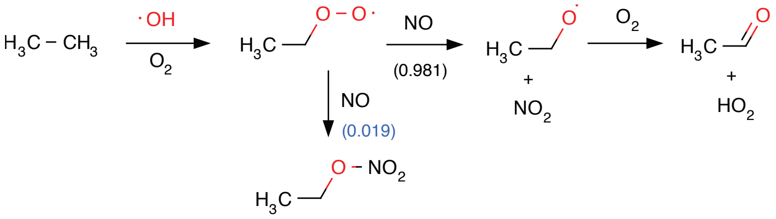

Figure B1. Ethane oxidation by OH radical in the presence of NO.

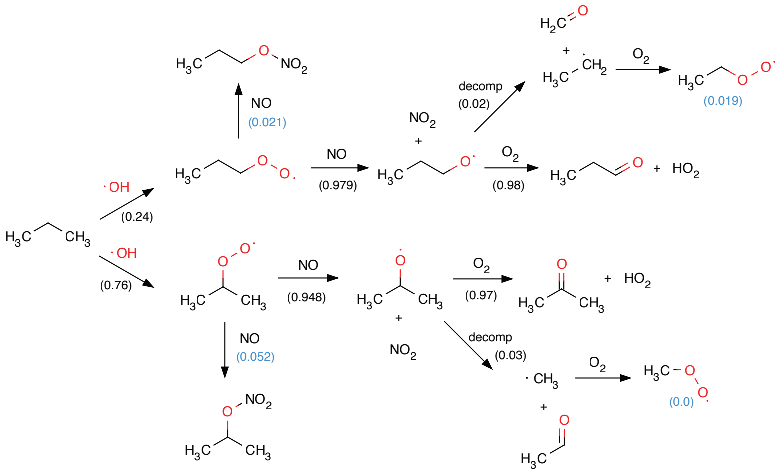

Figure B2. Propane oxidation by OH radical in the presence of NO.